Structure and Ligand Binding Properties of Myoglobins Reconstituted with Monodepropionated Heme: Functional Role of Each Heme Propionate Side Chain † , ‡

ARTICLE *in* BIOCHEMISTRY · SEPTEMBER 2007

Impact Factor: 3.02 · DOI: 10.1021/bi7007068 · Source: PubMed

8 AUTHORS, INCLUDING:

Masatomo Makino
Shimane Institute for Industrial Technology
18 PUBLICATIONS **330** CITATIONS
SEE PROFILE

Shun Hirota
Nara Institute of Science and Technology
172 PUBLICATIONS **3,136** CITATIONS
SEE PROFILE

Yoshio Hisaeda
Kyushu University
250 PUBLICATIONS **3,714** CITATIONS
SEE PROFILE

Structure and Ligand Binding Properties of Myoglobins Reconstituted with Monodepropionated Heme: Functional Role of Each Heme Propionate Side Chain[†,‡]

Katsuyoshi Harada,[§] Masatomo Makino,[||] Hiroshi Sugimoto,[⊥] Shun Hirota,[@,Δ,◇] Takashi Matsuo,[§] Yoshitsugu Shiro,[⊥] Yoshio Hisaeda,[+] and Takashi Hayashi*[,§,#]

Department of Applied Chemistry, Graduate School of Engineering, Osaka University, Suita 565-0871, Japan, Graduate School of Life Science, University of Hyogo, Ako 678-1297, Japan, Department of Physical Chemistry and 21 Century COE Program, Kyoto Pharmaceutical University, Kyoto 607-8414, Japan, PRESTO, JST, Saitama 332-0012, Japan, Harima Institute, RIKEN SPring-8 Center, Sayo 679-5148, Japan, Department of Chemistry and Biochemistry, Graduate School of Engineering, Kyushu University, Fukuoka 819-0395, Japan, Institute for Molecular Science, Okazaki 444-8787, Japan

Received April 14, 2007; Revised Manuscript Received June 7, 2007

ABSTRACT: Two heme propionate side chains, which are attached at the 6 and 7 positions of the heme framework, are linked with Arg45 and Ser92, respectively, in sperm whale myoglobin. To evaluate the role of each propionate, two kinds of one-legged hemins, 6-depropionated and 7-depropionated protohemins, were prepared and inserted into the apomyoglobin to yield two reconstituted proteins. Structural data of the reconstituted myoglobins were obtained via an X-ray crystallographic analysis at a resolution of 1.1−1.4 Å and resonance Raman spectroscopy. It was found that the lack of the 6-propionate reduces the number of hydrogen bonds in the distal site and clearly changes the position of the Arg45 residue with the disrupting Arg45−Asp60 interaction. In contrast, the removal of the 7-propionate does not cause a significant structural change in the residues of the distal and proximal sites. However, the resonance Raman studies suggested that the coordination bond strength of the His93−Fe bond for the protein with the 7-depropionated protoheme slightly increases compared to that for the protein with the native heme. The O_2 and CO ligand binding studies for the reconstituted proteins with the one-legged hemes provide an important insight into the functional role of each propionate. The lack of the 6-propionate accelerates the O_2 dissociation by ca. 3-fold compared to those of the other reconstituted and native proteins. The lack of the 7-propionate enhances the CO affinity by 2-fold compared to that of the protein with the native heme. These results indicate that the 6-propionate clearly contributes to the stabilization of the bound O_2, whereas the 7-propionate plays an important role in the regulation of the Fe−His bond.

Protoheme IX (heme b), one of the prosthetic groups in a series of hemoproteins, is tightly bound in the protein matrix by multiple noncovalent interactions. For the O_2-binding hemoproteins, such as myoglobin and hemoglobin, the heme[1] is stabilized by Fe−His coordination, hydrophobic contact of the heme with several nonpolar aliphatic and aromatic amino acid residues, and the formation of a a salt bridge between the heme propionate side chains and polar amino acid residues near the entrance of the heme pocket (*1*). Structures of the proteins determined by an X-ray crystallographic analysis and a NMR spectroscopic study of the myoglobin clearly showed the heme−globin interaction. In addition, the kinetic and thermodynamic studies of the heme binding to the apoprotein have provided important insight into the understanding of the contribution of each interaction to the stabilization of the heme−globin complex (*2*). It is known that the overall binding affinity of apomyoglobin for hemin is approximately 10^{12}−10^{14} M^{-1}, and the propionate−amino acid residue interactions contribute a factor of 10^2−10^4 M^{-1} to the overall affinity. In particular, the previous kinetic studies of the dissociation of heme from horse heart myoglobin suggest that the interactions between the two heme propionate side chains and polar amino acids such as Lys45, Ser92, and His97 contribute to the stabilization of the heme molecule in the globin (*3*). Our next goal has been to elucidate the relationship between the heme−globin interaction and its physiological function (*4* and references cited therein).

The three-dimensional (3D) structural analysis of sperm whale myoglobin indicates that the two propionate side

[†] This study was supported by a Grant-in-Aid for Scientific Research from the Ministry of Education, Culture, Sports, Science and Technology. K.H. thanks the Japan Society for the Promotion of Science (JSPS) for the financial support.

[‡] Refined coordinates and structure factors have been deposited in the Protein Data Bank (entries 2EKT and 2EKU for aquometmyoglobins reconstituted with 6-depropionated and 7-depropionated protohemin IX species, respectively).

* To whom correspondence should be addressed: Department of Applied Chemistry, Osaka University, Suita 565-0871, Japan. Phone and fax: +81-6-6879-7928. E-mail: thayashi@chem.eng.osaka-u.ac.jp.

[§] Osaka University.

[||] University of Hyogo.

[⊥] RIKEN SPring-8 Center.

[@] Kyoto Pharmaceutical University.

[Δ] JST.

[◇] Present address: Graduate School of Materials Science, Nara Institute of Science and Technology, Ikoma 630-0192, Japan.

[+] Kyushu University.

[#] Institute for Molecular Science.

[1] Abbreviations: heme, protoheme IX; hemin, ferric protoheme IX; rMb, reconstituted myoglobin.

10.1021/bi7007068 CCC: $37.00
Published on Web 07/18/2007

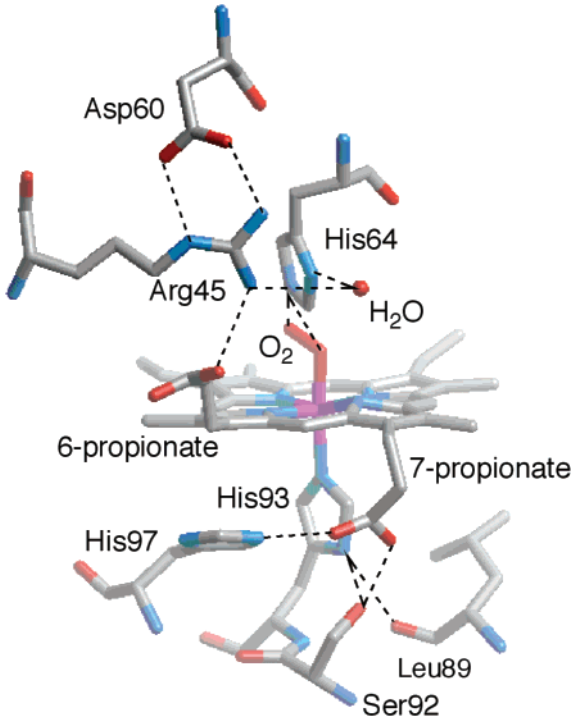

FIGURE 1: Hydrogen bonding network in the proximal and distal sites of sperm whale oxymyoglobin (1MBO).

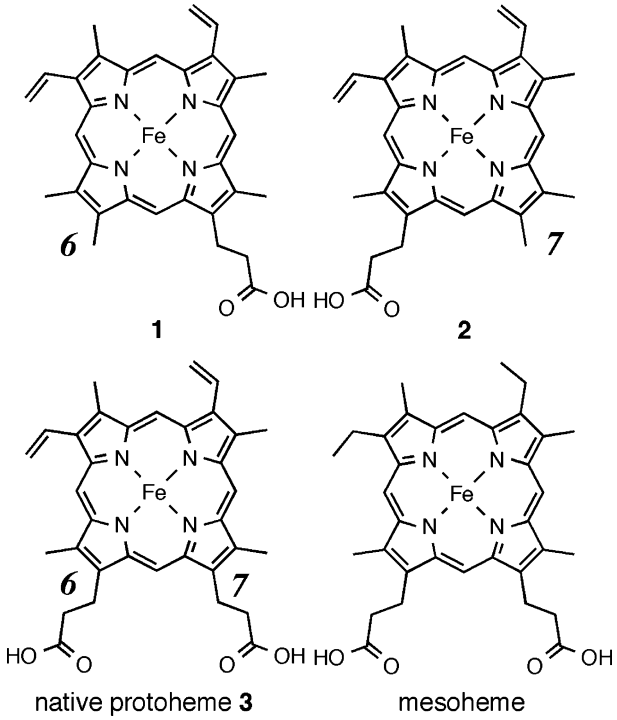

FIGURE 2: Structures of one-legged hemes **1** and **2**, protoheme IX **3**, and mesoheme.

chains linked at the 6 and 7 positions of the heme framework interact with Arg45 and Ser92/His97, respectively. According to the crystal structure of oxymyoglobin as shown in Figure 1, it displays two unique networks (*5*, *6*). One is the distal site network of the 6-propionate-Arg45-H_2O-His64-bound O_2. The other is the proximal site network of 7-propionate-Ser92-His93. These hydrogen bonding networks seem to be essential to regulation of the myoglobin function, because the former network stabilizes the bound O_2 and the latter may control the position of the imidazole ring as an axial ligand of His93. Although it is unambiguous that each heme propionate side chain is a part of the hydrogen bonding networks, their contribution to the myoglobin function has not been completely determined.

Several groups have devoted their efforts to evaluating the role of the propionate−globin interaction in protein function by a mutagenetic approach, in which the propionate-bound amino acid residues, such as Arg45 and Ser92, were replaced with a different type residue. For example, residue 45 was substituted with noncharged residues, such as Ser or Gly (*7*, *8*). The 3D structure of the aquomet K45S mutant for pig myoglobin revealed that the mutation produces only a small deviation in the α-carbon main chain from that of the native protein, but a more open pocket structure compared to that of the native myoglobin, although a significant change in the kinetic parameters for O_2 or CO binding was not observed for these mutants. On the other hand, the replacement of Ser92 with Val or Leu for the pig myoglobin increased the ligand binding affinities, indicating that the removal of the Ser92−His93 hydrogen bond activates the heme iron for the ligand binding (*9*), whereas the S92A mutants for human and pig myoglobin show approximately the same kinetic parameters with the corresponding native myoglobin (*9*, *10*). Furthermore, several groups have reported the structural data of position 92 mutants to elucidate the contribution of Ser92 to the myoglobin function (*9*−*11*). However, it is still not clear that the real role of the interaction between the 7-propionate and Ser92 has an influence on ligand binding.

Another strategy for evaluating the role of the two heme propionate side chains in ligand binding in myoglobin will be the removal of one of the propionates by chemical modification. Although a simple idea is the esterification of one of the heme propionate side chains to disrupt the hydrogen bonding network, it is difficult to selectively prepare the hemin monoester at the position 6 or 7 side chain by organic synthesis (*7*, *12*). To overcome this problem, we first prepared two "one-legged" mesohemin derivatives in which the 6- or 7-propionate side chain was replaced with a methyl group and then inserted them into the apomyoglobin (*13*). The two proteins reconstituted with each mesoheme derivative produced kinetic parameters for ligand binding events different from those observed by the native protein. However, these reconstituted myoglobins were not appropriate for the exact evaluation of the role of each propionate side chain on the basis of the kinetic studies, because there are two heme orientations, forward and backward, in the asymmetric heme pocket with a ratio of 4−8. In contrast, La Mar, Smith, and their co-workers reported that two myoglobins, rMb(**1**) and rMb(**2**), reconstituted with the prototype one-legged protohemins, **1** and **2**, respectively, as shown in Figure 2, mainly give the forward hemin plane conformation in the heme pocket (*14*, *15*). According to their studies, the ratios of the forward and backward hemin planes in the sperm whale myoglobin were determined to be 20:1 and 18:1 for rMb(**1**) and rMb(**2**), respectively, by a ^{1}H NMR technique. Therefore, rMb(**1**) and rMb(**2**) will be suitable for understanding how each heme propionate influences the myoglobin function, although, to the best of our knowledge, the O_2 binding properties for rMb(**1**) and rMb(**2**) have never been reported in previous reports (*16*, *17*).

Recently, we prepared **1** and **2** by Smith's modified synthetic method (*18*). The structures of the reconstituted proteins, rMb(**1**) and rMb(**2**), were evaluated by a Raman spectroscopic method and an X-ray crystallographic analysis. Moreover, the kinetic parameters of O_2 and CO binding for the two reconstituted myoglobins were compared to those of the myoglobin rMb(**3**) with the native protoheme IX (**3**). On the basis of these results, it was found that the 6-propionate side chain is crucial for stabilization of the O_2 complex, whereas the CO binding is affected by the removal of the 7-propionate side chain. In this paper, we summarize the structure and physicochemical properties of the myoglobins reconstituted with the one-legged hemes and discuss the role of each heme propionate side chain in ligand binding events.

EXPERIMENTAL PROCEDURES

Instruments. The UV−visible experiments were conducted using a Shimadzu UV-3150 double-beam spectrophotometer equipped with a thermostated cell holder with a 0.1 °C deviation. Purification of the proteins was performed with an Amersham Biosciences ÄKTA FPLC system with a Frac-920 fraction collector at 4 °C. The mass analysis of the myoglobins was carried out using a TOF mass spectrometer equipped with electrospray ionization on an Applied Biosystems Mariner API-TOF workstation. The spectroelectrochemical measurement was performed by regulating the potentials using a Hokuto Denko HA-305 potentiostat/galvanostat. The IR spectra of the CO-ligated Mbs were recorded using a JASCO FT/IR-620 spectrometer. The equipment for resonance Raman spectroscopy and X-ray crystallographic analysis is described below. Kinetic measurements of O_2 and CO binding were carried out using a stopped-flow/laser-flash photolysis system constructed by Unisoku, Co., Ltd. (Osaka, Japan). A Xe arc lamp was employed as the source of the probe light to follow the spectral changes. For laser-flash photolysis, a sample was excited with 5 ns pulses (532 nm) from a Q-switched Nd:YAG laser (Surelite I, Continuum). The pH values were monitored with a Beckman Φ71 pH meter.

Materials. The native sperm whale myoglobin was purchased from Biozyme Laboratories, Ltd. All reagents of the highest guaranteed available grade were obtained from commercial sources and were used as received unless otherwise indicated. Distilled water was demineralized with a Millipore Milli-Q Academic A10 apparatus. The proteins were purified by column chromatography through a CM-52 (Whatman), Sephadex G-25 (Amersham Biosciences), Hi-Trap Desalting (Amersham Biosciences), and/or Superdex 75 (Amersham Biosciences) column. The one-legged hemins **1** and **2** were synthesized by the method described in a previous paper (*18*). The native protohemin IX (**3**) was purchased from Tokyo Chemical Industry Co., Ltd.

Protein Reconstitution with One-Legged Hemin. The sperm whale apomyoglobin was prepared from the native metmyoglobin by Teale's 2-butanone method (*19*). A solution of the apomyoglobin was prepared by dissolving lyophilized powder (8.6 mg) in chilled 100 mM potassium phosphate buffer (pH 7.0). A 1.2 equiv amount of the one-legged hemin was dissolved in pyridine (400 μL), and the mixture was added dropwise to the solution of apomyoglobin (ca. 40 mL). After being shaken for 1.5 h at 4 °C, the solution was dialyzed against 1 L of 100 mM potassium phosphate buffer (pH 7.0) for 12 h at 4 °C. After the mixture was centrifuged (3000 rpm for 20 min at 4 °C) and concentrated (ca. 0.5 mL), the solution was passed through a Sephadex G-25 column (1.5 cm × 30 cm) equilibrated in 100 mM potassium phosphate buffer (pH 7.0). The solution of a purified reconstituted myoglobin was concentrated (ca. 1 mM) and maintained at 4 °C.

Determination of Fe^{2+}/Fe^{3+} Redox Potentials. The spectroelectrochemical measurements were carried out at 25 °C under a N_2 atmosphere using an optically transparent thin-layer electrode cell (optical path length of 0.6 mm). A working electrode and a counter electrode made of Pt mesh were used along with a Ag/AgCl reference electrode. The potentials of these electrodes were controlled and measured with a Hokuto Denko HA-305 potentiostat/galvanostat. A solution of metmyoglobin (50 μM) was prepared in 100 mM potassium phosphate buffer (pH 7.0) containing $Ru(NH_3)_6Cl_3$ (100 μM, $E = 51$ mV vs NHE) as an electron mediator. A typical increment of 25 mV was applied to the system, and at each applied potential, the electronic absorption spectra were monitored until no change was detected due to the establishment of equilibrium. The spectra of the fully reduced and fully oxidized myoglobins were obtained by applying the potentials of −500 and +200 mV versus Ag/AgCl. The data were fitted to the Nernst equation, and the resulting midpoint of the redox potential was referenced to the normal hydrogen electrode (NHE).

Resonance Raman Spectroscopy. A 25 μL solution of 0.4 mM metmyoglobin in 100 mM potassium phosphate buffer (pH 7.0) was transferred to an airtight spinning cell. The solution was diluted with 65 μL of 100 mM potassium phosphate buffer (pH 7.0), and three repeated evacuations of the gas inside the cell were followed by the introduction of N_2. A small amount of a N_2-saturated dithionite solution (10 mM, 10 μL) was added to prepare the deoxymyoglobin. The CO adduct of the myoglobin (CO-myoglobin) was formed through two repeated evacuations of the gas inside the cell followed by the introduction of N_2 and finally the incorporation of $^{12}C^{16}O$ (or $^{13}C^{18}O$) before a small amount (10 mM, 10 μL) of a N_2-saturated dithionite solution was added. The Raman scattering was excited at 441.6 nm (12 mW) by a He/Cd laser for the deoxymyoglobin and at 413.1 nm (10 mW) by a Kr^+ laser for the CO-myoglobin. The Raman shifts were calibrated with toluene and CH_2Cl_2.

IR Spectroscopy. The IR spectra of the CO-myoglobins were recorded with a JASCO FT/IR-620 spectrometer with a 1.0 cm^{-1} resolution for the frequency shift at room temperature. A cell using CaF_2 windows with a 0.1 mm optical path length was used. The background spectrum was collected for the corresponding deoxymyoglobins. The observed spectra were deconvoluted into two components with a half-width of 6 cm^{-1}.

Crystallization and Structure Determination. The purified protein in 10 mM phosphate buffer (pH 7.0) was concentrated by centrifugation to 36 and 18 mg/mL for the met-rMb(**1**) and met-rMb(**2**) crystallizations, respectively. Crystals of the ferric form were grown using the sitting-drop vapor-diffusion method. A 1 μL protein solution was added to a 1 μL reservoir solution and equilibrated against a 100 μL reservoir solution. A crystal of met-rMb(**1**) was obtained in

Table 1: Data Collection and Refinement Statistics

	rMb(**1**)	rMb(**2**)
Data Collection		
X-ray source	SPring-8 BL44B2	SPring-8 BL45XU
detector	ADSC Quantum 210	RIGAKU R-axis V
wavelength (Å)	0.78	1.0
resolution (Å)	50−1.10 (1.14−1.10)	50−1.40 (1.45−1.40)
space group	*P*6	$P2_1$
unit cell parameters	$a = b = 90.2$ Å, $c = 45.3$ Å	$a = 63.8$ Å, $b = 30.5$ Å, $c = 34.4$ Å, $\beta = 105.5°$
no. of observations	2005844	167220
no. of unique reflections	85421	25369
completeness (%)	100 (100)	100 (99.7)
R_{sym} (%)	6.2 (34.9)	5.2 (32.0)
$I/\sigma(I)$	38.7 (6.8)	25.6 (6.8)
Refinement		
resolution (Å)	10−1.1	10−1.4
total no. of reflections	81016	24010
no. of non-H atoms		
protein	1264	1246
water	303	204
other	59	54
R_{cryst} (%)	13.3	12.7
R_{free} (%)	15.8	19.5
rmsd from target		
bond lengths (Å)	0.014	0.014
angle distances (Å)	0.030	0.030
mean isotropic equivalent		
B-factor (Å^2)		
all protein atoms	12.8	14.6
main chain atoms	10.3	11.7
side chain atoms	15.4	17.4
water molecules	26.9	27.6
protoheme	8.6	10.0
sulfate ions	29.0	17.6

3.0 M ammonium sulfate and 0.1 M Bis-Tris-propane at pH 6.4 and 4 °C. The crystal of met-rMb(**2**) was obtained in 3.1 M ammonium sulfate and 0.1 M Bis-Tris-propane at pH 6.4 and 17 °C. The crystals were soaked in cryoprotectant solution (10% glucose and 10% xylitol in reservoir solution) and flash-frozen in liquid nitrogen. The X-ray diffraction data were collected at BL44B2 or BL45XU in SPring-8, Hyogo, Japan. The data were integrated and merged using HKL2000 (*20*). The data collection and refinement statistics are listed in Table 1. The initial phases of the rMb(**1**) and rMb(**2**) crystals were obtained by the molecular replacement method using the native myoglobin (PDB entry 1JW8 or 1A6K) as a search model. The 5% randomly selected reflections were selected as test reflections for use in the free *R* cross-validation method throughout the refinement (*21*). The initial model was refined by simulated annealing using CNS (*22*). The multiple rounds of manual model rebuilding and positional and individual *B*-factor refinements allowed placement of the water molecules and assignment of some alternate side chain conformations. The solvent molecules were included, if they had a good stereochemistry and reasonable density in the $F_o - F_c$ and $2F_o - F_c$ map. Subsequent refinement was performed with SHELXL (*23*). All the hydrogen atoms were added according to the geometrical criteria. After introduction of anisotropic *B*-factors, further alternate conformations and water molecules could be modeled. The initial run of SHELX was performed using the parameter of the heme group of 1A6K for the protoheme of rMb(**1**) or rMb(**2**). The restraints on the protoheme were gradually removed, and the final stages of refinement restrained only the bond length and bond angles of the propionate as previously described (*6*). The root-mean-square deviations in the superposition were calculated for 140 pairs of Cα atoms of residues 2−116 and 124−148 using LSQKAB (*24*), because the structures of the N- and C-terminal residues are flexible and the structure of residues 117−123 (GH corner) has a high pH dependency, as reported by Yang *et al.* (*25*). The figures were created with Pymol, Molscript, and Raster3D (*26*−*28*).

O_2 Binding of Myoglobins. The oxymyoglobins were prepared by exposure of the deoxy form to air. The formation of the oxygenated form was confirmed by the UV−vis spectral changes. The association of O_2 was observed by the absorbance change at 435 nm after flash photolysis of the oxy form under 1 atm of O_2 at 25 °C. The time course of the absorbance was analyzed by single-phase kinetics to give the pseudo-first-order rate constant. By dividing this value by the O_2 concentration (2.64×10^{-4} M), we obtained the association rate constant. The dissociation of O_2 was assessed by following the UV−vis spectral changes after rapidly mixing the oxygenated form with excess $K_3[Fe(CN)_6]$ using a stopped-flow apparatus. The O_2 affinity was calculated from the ratio of the association and dissociation rates.

CO Binding of Myoglobins. The CO-myoglobins were obtained by reduction with a slight excess of sodium dithionite under a CO atmosphere. The formation of the CO-bound form was confirmed by the UV−vis spectral changes. The associations of CO were observed by the absorbance change at 423 nm after flash photolysis of the CO form under 1 atm of CO at 25 °C. The time course of the absorbance

Table 2: Absorption Maxima for Myoglobins[a]

	λ_{max} (nm)			
protein	met-Mb	deoxy-Mb	oxy-Mb	CO-Mb
rMb(**1**)	408, 503, 630	432, 557	417, 543, 581	422, 541, 577
rMb(**2**)	407, 504, 630	431, 557	417, 542, 580	421, 541, 576
rMb(**3**)	408, 504, 630	432, 557	417, 543, 581	422, 541, 577

[a] pH 7.0 (100 mM phosphate buffer) and 25 °C.

was analyzed by single-phase kinetics to give the pseudo-first-order rate constant. By dividing this value by the CO concentration (9.85×10^{-4} M), we obtained the association rate constant. The extents of dissociation of CO from the CO-bound myoglobins were measured by displacement with NO. A solution of the CO-bound myoglobins was mixed with the NO-saturated buffer by a stopped-flow apparatus, and the decrease in absorbance at 423 nm was monitored at 25 °C.

Autoxidation for Oxygenated Myoglobins. Autoxidations for the oxygenated myoglobins were monitored by absorbance changes in the range of 500−700 nm every 8 min for oxygenated rMb(**1**) and every 40 min for the oxygenated rMb(**2**) and rMb(**3**) at 37 °C under aerobic conditions. The time course of the absorbance at 580 nm was analyzed by first-order kinetics to afford the autoxidation rate.

RESULTS

Preparation and Characterization of Reconstituted Myoglobins. Insertion of hemins **1**−**3** into the sperm whale apomyoglobin was carried out by a conventional method. In a series of our studies except for the X-ray crystallographic analysis, we used the myoglobin rMb(**3**) reconstituted with the native prosthetic group, protohemin IX (**3**), as the reference protein instead of the native myoglobin, because of the reducing experimental artifacts. The ESI-TOF mass spectroscopy measurement of the reconstituted ferric proteins showed the corresponding desired mass numbers of 17 760.8 and 17 760.3 for rMb(**1**) and rMb(**2**), respectively. The reconstituted ferrous myoglobins were obtained by dithionite reduction. The reversibility of the O_2 and CO bindings for the deoxymyoglobins is similar to those observed in the native myoglobin and rMb(**3**). The spectra of a series of rMb(**1**)s are exactly the same as those for the native myoglobin and rMb(**3**). In contrast, the Soret bands of met-rMb(**2**), deoxy-rMb(**2**), and CO-rMb(**2**) were always shifted by 1 nm compared to those of the native myoglobin and rMb(**3**) with a good reproducibility, suggesting that the removal of the 7-propionate side chain slightly perturbs the electronic structure of the heme plane. The absorption maxima for the various species of the myoglobins are summarized in Table 2.

Fe^{2+}/Fe^{3+} Redox Potentials. Figure 3 shows the results of the spectroelectrochemical measurements using the thin-layer cell with Pt mesh in the presence of $Ru(NH_3)_6Cl_3$ as an electron mediator. The potentiometric titrations for rMb(**1**) and rMb(**2**) gave similar spectral changes from the ferrous to ferric states to the reference protein rMb(**3**). All proteins exhibited an electrochemically reversible behavior as observed for the native protein between +422 and −278 mV (vs NHE). Table 3 summarizes the Fe(II)/Fe(III) redox potentials which were determined by the linear Nernst plots

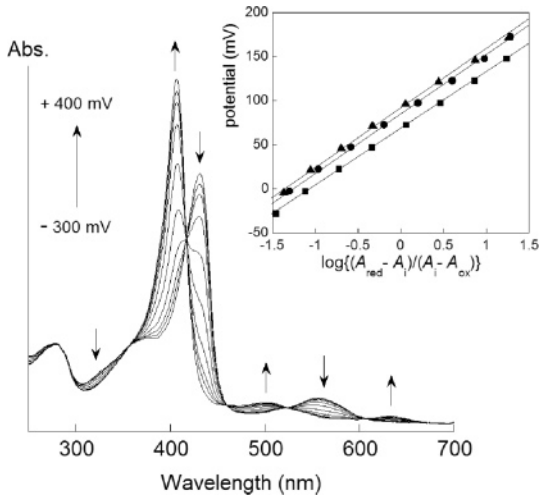

FIGURE 3: UV−vis spectra of rMb(**1**) at various applied potentials (vs NHE) during the spectroelectrochemical titration in 100 mM potassium phosphate buffer (pH 7.0) at 25 °C under N_2. The inset is a Nernst plot obtained from the spectral changes at 433 nm of rMb(**1**) (▲), rMb(**2**) (●), and rMb(**3**) (■).

Table 3: Physicochemical Parameters for Metmyoglobins

protein	pK_a[a]	$E_{1/2}$ (mV, vs NHE)[b]
rMb(**1**)	8.67 ± 0.03	91.7 ± 1.0
rMb(**2**)	8.73 ± 0.03	84.6 ± 1.0
rMb(**3**)	8.95 ± 0.03	70.0 ± 0.4

[a] Acid−alkaline equilibrium constants of a heme-bound water molecule, in 100 mM KCl at 25 °C. [b] Redox potentials, Fe(III)/Fe(II). At pH 7.0 and 25 °C.

as shown in the inset of Figure 3. On the basis of the results, it is clear that the removal of the propionates positively shifts the values. One of the main reasons is due to the removal of one negative charge at the terminus of the propionate side chain (*12*). In particular, the redox potential of rMb(**1**) is positively shifted by 22 mV compared to that of rMb(**3**), indicating that the lack of the 6-propionate side chain enhances the electron acceptability of the heme iron.

Resonance Raman Spectra of Deoxymyoglobins. The heme in myoglobin is attached to the polypeptide chain only through the coordination between His93 and the heme iron. Thus, the nature of the Fe−His93 bond provides valuable information about the reactivity of the heme. In particular, it is well-known that the resonance Raman (RR) spectroscopy is a useful technique for evaluating the coordination property of the heme iron (*29*). Figure 4 displays the RR spectra in the 180−330 cm^{-1} region for the reconstituted deoxymyoglobins with a 0.25 cm^{-1} resolution for the frequency shift at room temperature (*29*, *30*). The RR spectrum of rMb(**1**) is definitely close to that of the reference protein rMb(**3**), whereas the ν(Fe−His) Raman band at 221 cm^{-1} for rMb(**2**) is slightly shifted to a higher wavenumber by 1 cm^{-1} compared to that of rMb(**3**). This finding suggests that the lack of the 7-propionate side chain has a slight influence on strengthening the coordination between the heme iron and the imidazole ring of His93.

Crystal Structure of Reconstituted Myoglobins. The X-ray crystal structures of the hexagonal form of met-rMb(**1**) and the monoclinic form of met-rMb(**2**) have been determined at resolutions of 1.1 and 1.4 Å, respectively. They were crystallized in the aquomet form. The coordinate errors of

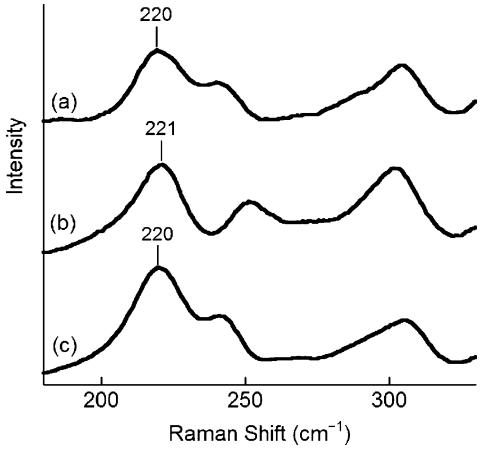

FIGURE 4: Resonance Raman spectra of deoxymyoglobins in the 180−330 cm^{-1} region in 100 mM potassium phosphate buffer (pH 7.0) at room temperature: (a) rMb(**1**), (b) rMb(**2**), and (c) rMb(**3**). The excitation wavelength was 441.6 nm with a laser power of 12 mW.

the structure of rMb(**1**) and rMb(**2**) are estimated from the Luzzati plot to be 0.06 and 0.08 Å, respectively (*31*). Figure 5 shows that the imidazole of His93 is linked to the Fe(III) atom of protohemin as a fifth ligand, and the water molecule is bound as a sixth ligand, as observed in the aquomet form of the native myoglobin. The electron density maps for the protohemin derivatives did not display an expanded shape of the methyl groups at the 1 and 3 positions of pyrrolic β-carbons. The density of the vinyl groups is very clear to show the peaks for the hydrogen atom in the $F_o - F_c$ map (not shown). These findings suggest the homogeneity of the protohemin orientation. The orientation and position of the protohemin derivatives and the torsion angles of the remaining propionate side chain are also conserved.

In a detailed comparison, when the structure of rMb(**1**) was superimposed on that of the native myoglobin (1A6K) of the monoclinic crystal using the 140 Cα atoms, the root-mean-square deviation (rmsd) is 0.38 Å (*6*). Because rMb(**1**) was crystallized in a hexagonal system, the rmsd value falls to 0.25 Å in the superposition onto the hexagonal (recombinant) native myoglobin (2MBW) (*32*). After the structure superposition, the plane of the 6-depropionated protohemin of rMb(**1**) and hemin of the native myoglobin (1A6K) is nearly parallel, and the deviation of the coordinate of the iron atom is 0.23 Å (Figure 5a). The other geometric parameters of **1** are summarized in Table 4. It should be noted that, among the number of sperm whale myoglobin structures in the Protein Data Bank, the hexagonal crystals have been obtained only for the recombinant myoglobin which was expressed in *Escherichia coli*. Since the hexagonal crystal has a large solvent fraction of 59%, the structure of the polypeptide seems to be sensitive to the changes in the pH or temperature of the solvent (*25*). On the other hand, the monoclinic crystal, which is commonly obtained for the native protein form of the sperm whale, has a small solvent fraction of 33% and its polypeptide structure seems to be affected by the contact of the neighboring molecules. However, even though they have different crystal packings and different pHs, the structures of the native myoglobins in both crystal forms have a conserved structure of a hydrogen bonding network involving the heme propionate side chains, surrounding residues, and water molecules. Therefore, in Figure 6, the hydrogen bonding network around the protohemin derivatives of rMb(**1**) and rMb(**2**) is compared to that of the native protein (1A6K).

The distal hydrogen bonding network of rMb(**1**) has a significant change, since the 6-propionate side chain of the native protein is directed to the distal site to create the salt bridge with the side chains of Arg45 (Figure 6a). Lack of the 6-propionate side chain causes a 2 Å shift in Arg45 so that it is close to the protohemin plane and disrupts the bridge between Arg45 and Asp60 **(**Figure 6b**)**. Furthermore, the hydrogen bonding network of the 6-propionate side chain and four waters (1024, 1058, 1102, and 1149), which have been detected in the native protein (Figure 6a), are replaced by a row of three waters (16, 239, and 165) in rMb(**1**). These changes might affect the water-mediated interaction between the hemin and main chain of the CD loop (Arg45 N, Asp44 N, and Lys42 O). On the other hand, the structure of the remaining 7-propionate and the hydrogen bonding network of the surrounding waters and protein residues are well-conserved in rMb(**1**).

The crystals of rMb(**2**) and native myoglobin (PDB entry 1A6K) are monoclinic and have very similar unit cell dimensions. These polypeptide structures can be superimposed well with a rmsd of 0.14 Å. The deviation of iron atoms after the superposition is as little as 0.04 Å **(**Figure 5b**)**. They have very similar side chain torsion angles and positions in the distal His64 and the proximal His93. The 7-propionate side chain of the native protein is directed to the proximal site and interacts with Ser92, His97, and three waters (1033, 1059, and 1118) (Figure 6a). Comparison of the distal site of the heme pocket between the native myoglobin and rMb(**2**) (panels a and c of Figure 6) shows no significant structural change in the remaining 6-propionate and hydrogen bonding network. The hydrogen bonding network of the proximal site of rMb(**2**) also exhibits a similar hydrogen bonding network, since the room generated by the lack of the 7-propionate side chain is filled by the two waters which mimic the O atoms of the propionate side chain that maintains the hydrogen bonds with His97, Ser92, and Wat1033 [Wat58 of rMb(**2**)]. The only difference is that the proximal side of rMb(**2**) cannot order four waters, including Wat1118 and Wat1059 that have been bound to Ser92 in the native protein.

O_2 and CO Binding. As one can clearly see in Table 5, the rate constants of the O_2 association for rMb(**1**) and rMb(**2**) are close to that observed for the reference protein rMb(**3**), whereas the dissociation of the O_2 ligand from oxy-rMb(**1**) is approximately 3 times faster than those for rMb(**2**) and rMb(**3**). Furthermore, the autoxidation for oxy-rMb(**1**) is also accelerated, suggesting that the oxygenated rMb(**1**) is less stable rather than those for rMb(**2**) and rMb(**3**). The CO binding behavior of the reconstituted myoglobins is different with the O_2 binding as shown in Table 6. The CO dissociation for rMb(**1**) is 1.3-fold faster than that for rMb(**3**). In contrast, rMb(**2**) shows a slightly higher rate constant for CO association and a lower constant for CO dissociation, indicating that the affinity of rMb(**2**) for CO is approximately 2-fold higher than that of rMb(**3**). For the CO binding, the 7-propionate side chain may regulate the binding kinetics.

CO Binding Structure. To obtain further insight into the CO binding mechanism, the infrared (IR) and RR spectra of CO complexes were recorded (*33*). The Fe−C stretching

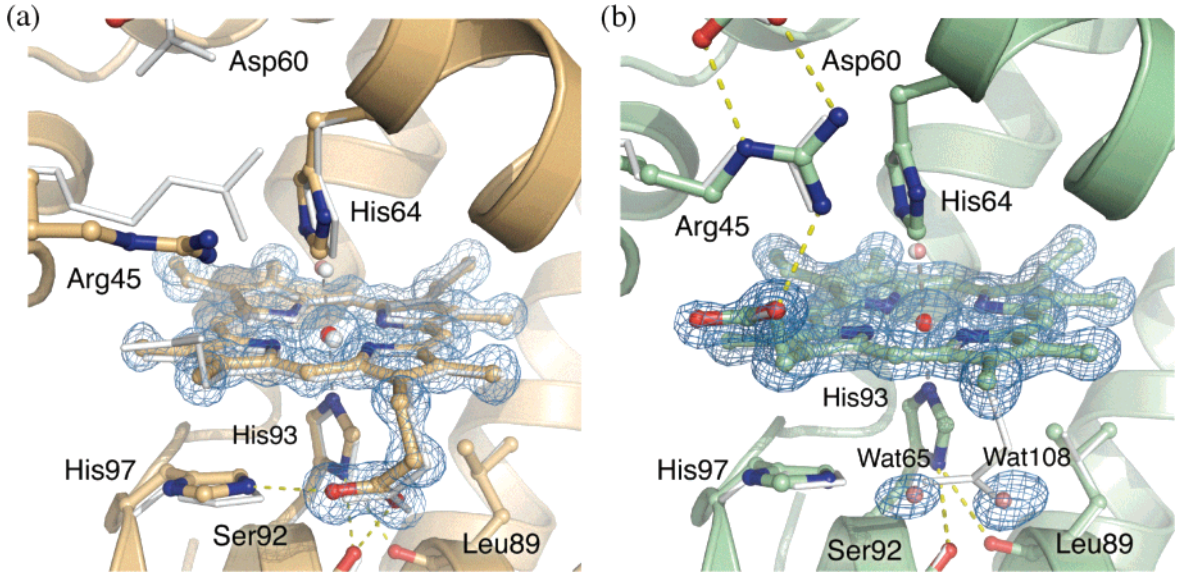

FIGURE 5: Crystal structure of two reconstituted myoglobins. The $2F_{obs} - F_{calc}$ electron density (1.0σ contours) around the one-legged hemin is also shown. (a) Superposition of rMb(**1**) (brown) and native protein (white; 1A6K) structures. (b) Superposition of rMb(**2**) (green) and native protein (white; 1A6K) structures.

Table 4: Geometry of One-Legged Hemins

	rMb(**1**)	rMb(**2**)	wild type (1A6K)
sample	aquomet	aquomet	aquomet
space group	*P*6	$P2_1$	$P2_1$
resolution (Å)	1.1	1.4	1.1
program	SHELXL	SHELXL	SHELXL
pH of crystal	6.4	6.4	7.0
rmsd of Cα atoms (Å)	0.38 (1A6K)	0.15 (1A6K)	
distance			
His64 Nε−Fe (Å)	4.38	4.37	4.30
Wat O−Fe (Å)	2.06	2.12	2.13
His93 Nε−Fe (Å)	2.03	2.05	2.14
Ser92 Oγ−His93 Nε (Å)	2.94	2.96	2.90
Leu89 O−His93 (Å)	3.05	3.08	2.97

modes for rMb(**2**) and the reference protein rMb(**3**) were exhibited at 511 cm^{-1}, which is 2 cm^{-1} higher than that of rMb(**1**), suggesting that the Fe−C bond for rMb(**1**) is weakened compared to that of the reference protein. The IR spectra in the region of the CO band for the myoglobins are shown in Figure 7. It is known that the IR spectrum of the CO-bound native protein exhibits two major peaks at 1945 cm^{-1} (A_1 conformer; 70%) and 1932 cm^{-1} (A_3 conformer; 30%) under physiological conditions, although there are at least four peaks in the region of 1900−2000 cm^{-1} (*34*, *35*). All proteins, rMb(**1**)−rMb(**3**), exhibit the similar main band (A_1) with the shoulder band (A_3), while the peak populations for the A_1 and A_3 conformers for CO−rMb(**1**) and CO−rMb(**2**) species are clearly different from those found for the reference protein, CO−rMb(**3**). Table 7 demonstrates that the population of the A_3 conformer band in rMb(**1**) is slightly smaller than that of rMb(**3**), whereas the population of the A_3 conformer band in rMb(**2**) is 2-fold larger than that observed for rMb(**3**). These findings suggest that each heme propionate side chain has an influence on the C−O bond strength for CO-myoglobin.

DISCUSSION

Role of Each Propionate Side Chain in Myoglobin Structure. The distal and proximal sites in the myoglobin have highly conserved hydrogen bonding networks formed by several amino acid residues and two heme propionate side chains. Much work has been done in understanding the structural and functional role of these networks by a variety of myoglobin mutants. In our previous study, we found that the one-legged hemins **1** and **2** were slightly unstable in the protein matrix under acidic conditions (*36*). The dissociation of hemin for rMb(**1**) and rMb(**2**) from the protein matrix occurs at pH 4.3−4.4, which is 0.2 pH unit higher than that observed for the native protein. The small differences in the $pK_{1/2}$ values between the native and reconstituted proteins may be derived from the lack of one propionate side chain. It is well-known that the stabilization of the heme in the protein matrix is mainly due to the Fe−His93 coordination and the hydrophobic contacts between the hemin and apolar amino acid residues, whereas the two heme propionate side chains are not tightly bound to the polar amino acid residues.

The structural data for the mutants with an unnatural residue at position 45 or 92 have been presented for evaluation of the physiological significance of the propionate−protein interaction. For example, the 3D structure of the K45S mutant of the pig myoglobin reveals that the mutation produces a more accessible ligand-binding pocket, whereas the overall structure of the mutant shows only small deviations from that observed for the wild-type protein. The high-resolution X-ray structure of rMb(**1**) demonstrates that the Arg45 residue swings away from the heme pocket to the bulk due to the removal of the 6-propionate side chain−Arg45 interaction. Additionally, the terminal carboxylate group in the Asp60 residue, which tightly interacts with Arg45 in the wild-type myoglobin, is also shifted to the outside because of the lack of a salt bridge with Arg45. Furthermore, the distal hydrogen bonding networks of rMb(**1**) cannot order the waters which have been mediated by the interaction between the CD loop and the heme in the native myoglobin. The finding suggests that a part of the CD loop and D helix regions may partially be loosened by the lack of the 6-propionate side chain with the disruption of the Arg45(CD3)−Asp60(E3) salt bridge.

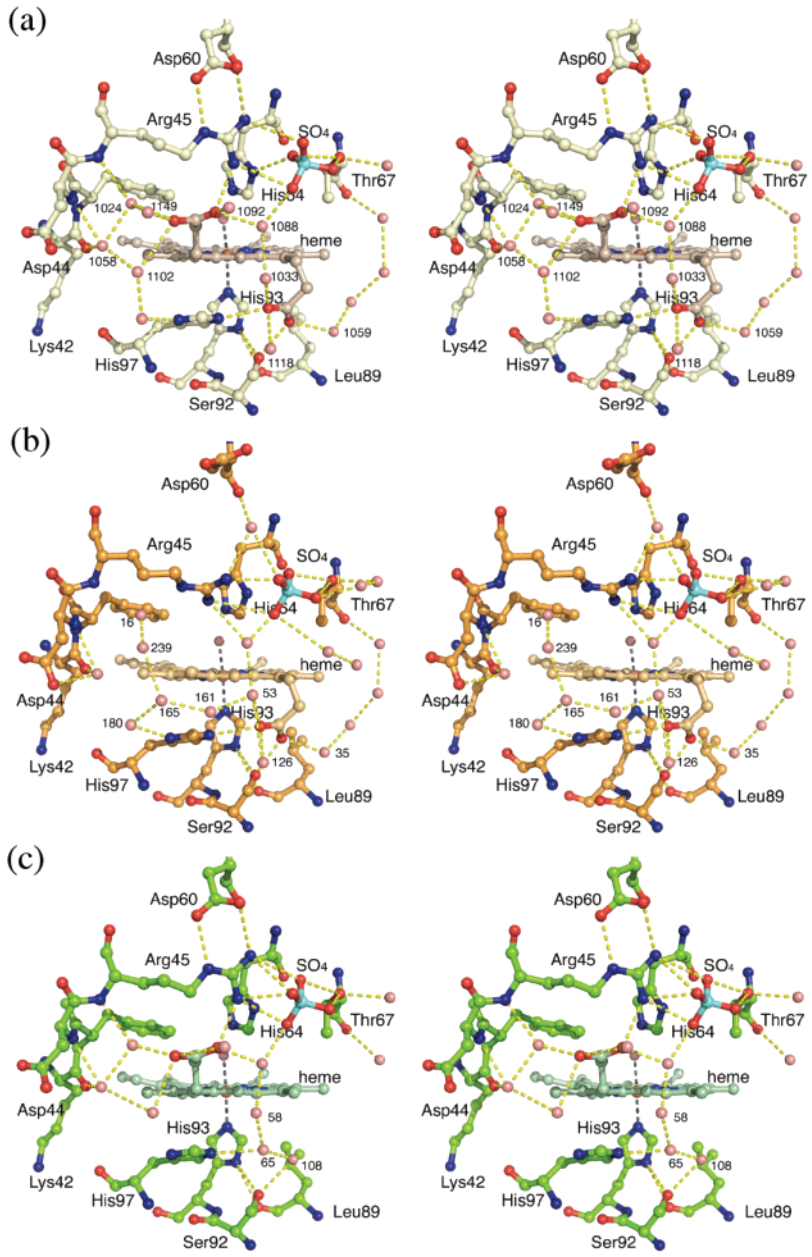

FIGURE 6: Stereoview of the heme pocket region in myoglobins: (a) native protein (1A6K), (b) rMb(**1**), and (c) rMb(**2**).

Table 5: O_2 Binding Parameters for Myoglobins[a]

protein	$k^{O_2}{}_{on}$ (μM^{-1} s^{-1})[b]	$k^{O_2}{}_{off}$ (s^{-1})[c]	K^{O_2} (M^{-1})[d]	k_{auto} (h^{-1})[e]
rMb(**1**)	19 ± 0.8	59 ± 1.9	3.2×10^5	0.58 ± 0.01
rMb(**2**)	19 ± 0.7	18 ± 0.6	1.1×10^6	0.13 ± 0.01
rMb(**3**)	18 ± 1.1	21 ± 0.6	8.6×10^5	0.10 ± 0.01

[a] pH 7.0 (100 mM phosphate buffer) and 25 °C. [b] Rate constants of O_2 association. [c] Rate constants of O_2 dissociation. [d] O_2 binding affinities are determined by the ratio of $k^{O_2}{}_{on}$ to $k^{O_2}{}_{off}$. [e] Rate constants for autoxidation from oxymyoglobin to metmyoglobin, at pH 7.0 (100 mM phosphate buffer) and 37 °C.

Table 6: CO Binding Parameters for Myoglobins[a]

protein	$k^{CO}{}_{on}$ (μM^{-1} s^{-1})[b]	$k^{CO}{}_{off}$ (s^{-1})[c]	K^{CO} (M^{-1})[d]	M'[e]
rMb(**1**)	0.58 ± 0.01	0.070 ± 0.002	8.3×10^6	26
rMb(**2**)	0.86 ± 0.01	0.044 ± 0.004	2.0×10^7	18
rMb(**3**)	0.63 ± 0.01	0.056 ± 0.003	1.1×10^7	13

[a] pH 7.0 (100 mM phosphate buffer) and 25 °C. [b] Rate constants of CO association. [c] Rate constants of CO dissociation. [d] CO binding affinities are determined by the ratio of $k^{CO}{}_{on}$ to $k^{CO}{}_{off}$. [e] K^{CO}/K^{O_2} ratio.

The X-ray crystallographic analyses of rMb(**1**) and rMb(**2**) at high resolution revealed no remarkable differences in the length of the hydrogen bonds of Ser92-His93 or Leu89-His93 (Table 4) which have been proposed to have a role in regulating the coordination geometry of the His93 imidazole. In general, the rotation of the imidazole ring in His93 is sensitive for the ^1H NMR spectroscopic measurement of the low-spin ferric state of myoglobin in the presence of KCN (metcyanomyoglobin). La Mar and his co-workers suggested that the heme-5-CH_3 resonance for metcyano-rMb(**2**) clearly shifted upfield at 23.8 ppm, whereas the 5-CH_3 proton signals of metcyano-rMb(**1**) and the corresponding native protein appeared at 26.9 and 26.1 ppm, respectively (*37*). Since it is well-known that a clear relationship exists between the angle of the His imidazole ring on the heme plane and the heme methyl chemical shift, it can be proposed that the removal of the 7-propionate side chain induces a slight deviation in

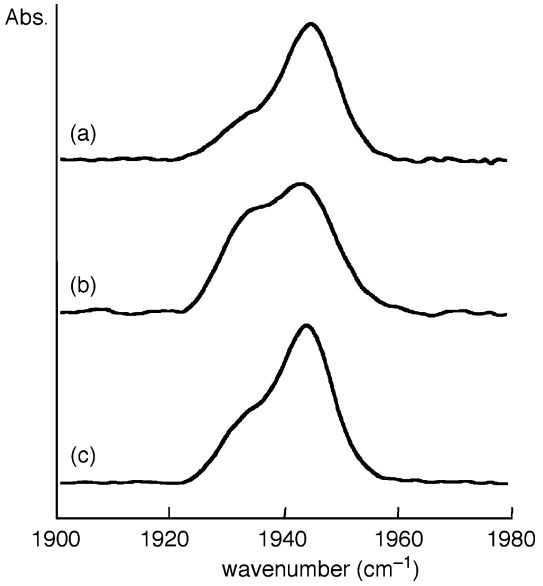

FIGURE 7: IR spectra of CO-bound myoglobins in the 1900−1980 cm^{-1} region in 100 mM potassium phosphate buffer (pH 7.0) at room temperature: (a) rMb(**1**), (b) rMb(**2**), and (c) rMb(**3**).

Table 7: IR Stretching Bands for CO-Myoglobins at Room Temperature and pH 7.0

protein	A_1 (cm^{-1})[a]	A_3 (cm^{-1})[a]
rMb(**1**)	1945 (83%)	1934 (17%)
rMb(**2**)	1943 (57%)	1933 (43%)
rMb(**3**)	1944 (74%)	1933 (26%)

[a] The populations of A_1 and A_3 bands in parentheses. These values were obtained by the deconvolution of each spectrum.

the His imidazole ring with a clockwise rotation of ∼5−10° on the porphyrin plane (*38*). Similar arguments may apply to the S92 mutants such as S92A and S92D (*10*, *11*). Furthermore, the RR spectra for deoxymyoglobin in the lower-frequency region are indicative of the feature of the Fe−His stretching mode. Friedman, Sligar, and their co-workers reported that the replacements of Leu89 and Ser92 with Ile and Ala, respectively, shifted the frequency of the ν(Fe−His) mode to a higher value by ∼3 cm^{-1} (*39*). The 1 cm^{-1} higher wavenumber shift of the corresponding frequency mode by removal of the 7-propionate side chain in rMb(**2**) is similar to those observed with the L89 and S92 mutants. This finding suggests that the 7-propionate side chain also plays an important role in the formation of the hydrogen bonding network to regulate the conformation and coordination property of the histidine imidazole ring.

Role of Each Propionate Side Chain in O_2 Binding. It is worth noting in the O_2 binding parameters that the dissociation of O_2 for oxy-rMb(**1**) is approximately 3-fold faster than that observed for rMb(**2**) and the reference protein rMb(**3**). This finding supports the fact that the lack of the 6-propionate side chain remarkably accelerated the dissociation of O_2 from oxy-rMb(**1**). As described above, there is a unique hydrogen bonding network, including the 6-propionate side chain and Arg45 and His64 residues, whereas the 3D structure of met-rMb(**1**) displays the deviation of the Arg45 residue. Thus, the lack of the 6-propionate side chain may have an influence on the conformation of the distal His64 which stabilizes the bound O_2, although a clear difference in the geometry of His64 imidazole rings between rMb(**1**) and the native protein was not seen. Olson and his co-workers reported that the replacement of Arg45 with Ser45 or Gly45 accelerated the O_2 dissociation 2.6- or 2.0-fold, respectively, compared to the native myoglobin (*7*). Both results clearly support the fact that the 6-propionate side chain and residue 45 are crucial units for fixing the imidazole ring of His64 in the best position to stabilize the bound O_2.

On the other hand, the O_2 dissociation of oxy-rMb(**2**) is slightly slower than that of rMb(**3**), and consequently, the affinity of rMb(**2**) for O_2 is the highest among three myoglobins. This result could be derived from the increase in the level of π-back-donation from the heme iron to dioxygen due to the increase in the strength of the His93−Fe coordination. The CO dissociation of CO-rMb(**2**) and CO-rMb(**3**) shows a similar behavior, and the stronger Fe−C bond and the weaker CO bond for CO-rMb(**2**) compared to the corresponding bonds of the CO complex of rMb(**3**) support an increase in the level of π-back-donation from the heme iron to the ligand (vide infra).

In addition, the 6-propionate−Arg45 interaction seems to inhibit the unfavorable autoxidation from the oxygenated protein to the inert aquomet species, because the oxidation of oxy-rMb(**1**) is 4.5- and 5.8-fold faster than that for oxy-rMb(**2**) and oxy-rMb(**3**), respectively, as shown in Table 5. Although the autoxidation mechanism is generally complicated (*40*−*42*), the findings suggest that the 6-propionate side chain clearly contributes to the stabilization of the oxygenated protein species.

The O_2 association rate constants for the reconstituted myoglobins, rMb(**1**) and rMb(**2**), are the same as that observed for rMb(**3**), indicating that the removal of the 6- or 7-propionate side chain has no drastic effect on the O_2 association. It has been reported that the changes in the O_2 association rate constants for the position 45 mutants are relatively small. These results suggest that the "wall" formed by the 6-propionate side chain and Arg45 via hydrogen bonding interaction may play a role in the inhibition of the entry of water molecules but does not act as a kinetic barrier to the entry of O_2 into the heme pocket (*43*).

Role of Each Propionate Side Chain in CO Binding. The kinetic parameters of the CO association and dissociation rate constants for rMb(**2**) are slightly different from those observed for rMb(**1**) and the reference protein rMb(**3**). These results indicate that the removal of the 7-propionate side chain enhances the CO affinity by 2-fold due to a small increase in the association rate constant and a small decrease in the dissociation rate constant for rMb(**2**). Although the changes in these parameters are not significant, these results show the same pattern that was observed for the S92A myoglobin mutant, in which the hydrogen bonding network in the proximal site is partially eliminated. It is known that the replacement of Ser92 with a nonpolar residue such as Ala allows flexibility of the proximal histidine, His93, because the S92A mutant lacks the characteristic hydrogen bonding network formed by the 7-propionate side chain and Ser92 and His93 (*9*, *10*). As a result, the imidazole ring of His93 in the S92A mutant can be rotated clockwise onto the porphyrin plane to reduce the steric hindrance between the pyrrole nitrogens, N2 and N4, and the axial imidazole carbons, Cδ and Cϵ, and then the affinity of S92A for CO is slightly increased. In the case of the CO binding for rMb-(**2**), the enhanced affinity with the fast k_{on} and slow k_{off} in

rMb(**2**) may also be derived from the increase in the structural flexibility of the proximal histidine because of the disruption of the characteristic hydrogen bonding network in the absence of the 7-propionate side chain. In addition, the IR spectra of the CO complex for rMb(**2**) reveal that the lack of the 7-propionate side chain increases in the population of the lower-frequency component (A_3 conformer) of the CO stretching modes at 1933 cm^{-1}. It is clearly indicative of the influence on the distal site with the enhanced π-back-donation from Fe to CO in CO-rMb(**2**). This structural evidence supports the fact that the hydrogen bonding interaction between the 7-propionate side chain and Ser92 regulates the conformation of the proximal histidine and the strength of the His93−Fe coordination. On the other hand, the weakness of the population of the A_3 band in CO-rMb-(**1**) suggests that the strength of the hydrogen bonding from the His64 NϵH group to the bound ligand is reduced in the distal site. In fact, the CO dissociation for CO-rMb(**1**) is slightly faster than that observed for the reference protein, CO-rMb(**3**). This finding also supports the fact that the removal of the 6-propionate side chain destabilizes the bound ligands.

CONCLUSIONS

In this study, we have demonstrated that the 6- and 7-propionate side chains work not only as a linker between the prosthetic group and globin but also as a regulator of the myoglobin function. Using the reconstituted myoglobins with two one-legged hemes in which the 6- or 7-propionate side chain was replaced with a methyl group, the roles of each propionate side chain in myoglobin were clarified. It is found that the lack of the 6-propionate side chain accelerated the O_2 dissociation and the autoxidation from the oxygenated heme. In addition, the crystallographic analysis indicated the deviation of Arg45 and Asp60 residues from the normal positions upon removal of the 6-propionate side chains. These findings support the facts that the 6-propionate side chain contributes to the formation of the stable hydrogen bonding network in the distal site and the increase in the strength of the hydrogen bond from the His64 NϵH atom to the heme-bound ligands. On the other hand, the lack of the 7-propionate side chain increases in the π-back-donation from the iron atom to CO, because the spectroscopic data suggest the slight conformational change of the His93 imidazole ring. According to the 3D structure of the native protein, the hydroxy group of Ser92 seems to be a pivot between the 7-propionate side chain and His93 imidazole. Thus, the 7-propionate side chain contributes to the regulation of the His93 conformation via Ser92 with the hydrogen bonding network in the proximal site. Finally, in this study, we estimated the structure of the deoxy- and oxymyoglobins from the extension of the obtained metmyoglobin structures. To precisely discuss the relationship between the ligand binding and structure of the proteins, further investigations into the structural analysis of the proteins are now underway.

ACKNOWLEDGMENT

We thank Professor Teizo Kitagawa (Okazaki Institute for Integrative Bioscience, National Institutes of Natural Science, Okazaki, Japan) for the use of the RR equipment. This paper is dedicated to the memory of late professor Yoshihiko Ito (Emeritus Professor of Kyoto University, Japan).

REFERENCES

1. Phillips, G. N., Jr. (2001) in *Handbook of Metalloproteins* (Messerschmidt, A., Huber, R., Poulos, T., and Wieghardt, K., Eds.) Vol. 1, pp 5−15, John Wiley & Sons, Chichester, U.K.
2. Hargrove, M. S., Barrick, D., and Olson, J. S. (1996) The association rate constant for heme binding to globin is independent of protein structure, *Biochemistry 35*, 11293−11299.
3. Hunter, C. L., Lloyd, E., Eltis, L. D., Rafferty, S. P., Lee, H., Smith, M., and Mauk, A. G. (1997) Role of the heme propionates in the interaction of heme with apomyoglobin and apocytochrome b_5, *Biochemistry 36*, 1010−1017.
4. Hayashi, T. (2005) in *Encyclopedia of Inorganic Chemistry 2* (King, B. R., Ed.) Vol. IV, pp 2167−2180, John Wiley & Sons, Chichester, U.K.
5. Phillips, S. E. V. (1980) Structure and refinement of oxymyoglobin at 1.6 Å resolution, *J. Mol. Biol. 142*, 531−554.
6. Vojtěchovský, J., Chu, K., Berendzen, J., Sweet, R. M., and Schlichting, I. (1999) Crystal structures of myoglobin-ligand complexes at near-atomic resolution, *Biophys. J. 77*, 2153−2174.
7. Carver, T. E., Olson, J. S., Smerdon, S. J., Krzywda, S., Wilkinson, A. J., Gibson, Q. H., Blackmore, R. S., Ropp, J. D., and Sligar, S. G. (1991) Contributions of residues 45(CD3) and heme-6-propionate to the bimolecular and geminate recombination reactions of myoglobin, *Biochemistry 30*, 4697−4705.
8. Oldfield, T. J., Smerdon, S. J., Dauter, Z., Petratos, K., Wilson, K. S., and Wilkinson, A. J. (1992) High-resolution X-ray structures of pig metmyoglobin and two CD3 mutants: Mb(Lys^{45}→Arg) and Mb(Lys^{45}→Ser), *Biochemistry 31*, 8732−8739.
9. Smerdon, S. J., Krzywda, S., Wilkinson, A. J., Brantley, R. E., Jr., Carver, T. E., Hargrove, M. S., and Olson, J. S. (1993) $Serine^{92}$-(F7) contributes to the control of heme reactivity and stability in myoglobin, *Biochemistry 32*, 5132−5138.
10. Shiro, Y., Iizuka, T., Marubayashi, K., Ogura, T., Kitagawa, T., Balasubramanian, S., and Boxer, S. G. (1994) Spectroscopic study of Ser92 mutants of human myoglobin: Hydrogen bonding effect of Ser92 to proximal His93 on structure and property of myoglobin, *Biochemistry 33*, 14986−14992.
11. Lloyd, E., Burk, D. L., Ferrer, J. C., Maurus, R., Doran, J., Carey, P. R., Brayer, G. D., and Mauk, A. G. (1996) Electrostatic modification of the active site of myoglobin: Characterization of the proximal Ser92Asp variant, *Biochemistry 35*, 11901−11912.
12. Lim, A. R., Sishta, B. P., and Mauk, A. G. (2006) Contribution of the heme propionate groups to the electron transfer and electrostatic properties of myoglobin, *J. Inorg. Biochem. 100*, 2017−2023.
13. Hayashi, T., Matsuo, T., Hitomi, Y., Okawa, K., Suzuki, A., Shiro, Y., Iizuka, T., Hisaeda, Y., and Ogoshi, H. (2002) Contribution of heme-propionate side chains to structure and function of myoglobin: Chemical approach by artificially created prosthetic groups, *J. Inorg. Biochem. 91*, 94−100.
14. La Mar, G. N., Pande, U., Hauksson, J. B., Pandey, R. K., and Smith, K. M. (1989) Proton nuclear magnetic resonance investigation of the mechanism of the reconstitution of myoglobin that leads to metastable heme orientational disorder, *J. Am. Chem. Soc. 111*, 485−491.
15. Santucci, R., Ascoli, F., La Mar, G. N., Pandey, R. K., and Smith, K. M. (1993) Reconstitution of horse heart myoglobin with hemins methylated at 6- or 7-positions: A circular dichroism study, *Biochim. Biophys. Acta 1164*, 133−137.
16. Gao, Y., El-Mashtoly, S. F., Pal, B., Hayashi, T., Harada, K., and Kitagawa, T. (2006) Pathway of information transmission from heme to protein upon ligand binding/dissociation in myoglobin revealed by UV resonance Raman spectroscopy, *J. Biol. Chem. 281*, 24637−24646.
17. Gao, Y., Koyama, M., El-Mashtoly, S. F., Hayashi, T., Harada, K., Mizutani, Y., and Kitagawa, T. (2006) Time-resolved Raman evidence for energy 'funneling' through propionate side chains in heme 'cooling' upon photolysis of carbonmonoxy myoglobin, *Chem. Phys. Lett. 429*, 239−243.
18. Smith, K. M., and Craig, G. W. (1983) Porphyrin synthesis through tripyrrins: An alternate approach, *J. Org. Chem. 48*, 4302−4306.
19. Teale, F. W. J. (1959) Cleavage of the haem-protein link by acid methylethylketone, *Biochim. Biophys. Acta 35*, 543.

20. Otwinowsky, A., and Minor, W. (1997) Processing of X-ray diffraction data collected in oscillation mode, *Methods Enzymol. 276*, 307−326.
21. Brünger, A. T. (1992) Free R value: A novel statistical quantity for assessing the accuracy of crystal structures, *Nature 355*, 472−475.
22. Brünger, A. T., Adams, P. D., Clore, G. M., DeLano, W. L., Gros, P., Grosse-Kunstleve, R. W., Jiang, J. S., Kuszewski, J., Nilges, M., Pannu, N. S., Read, R. J., Rice, L. M., Simonson, T., and Warren, G. L. (1998) Crystallography & NMR system: A new software suite for macromolecular structure determination, *Acta Crystallogr. D54*, 905−921.
23. Sheldrick, G. M., and Schneider, T. R. (1997) SHELXL: High resolution refinement, *Methods Enzymol. 277*, 319−343.
24. Collaborative Computational Project, Number 4 (1994) The CCP4 Suite: Programs for Protein Crystallography, *Acta Crystallogr. D50*, 760−763.
25. Yang, F., and Phillips, G. N., Jr. (1996) Crystal structures of CO-, deoxy- and met-myoglobins at various pH values, *J. Mol. Biol. 256*, 762−774.
26. DeLano, W. L. (2002) *The PyMOL Molecular Graphics System*, DeLano Scientific, San Carlos, CA.
27. Kraulis, P. J. (1991) MOLSCRIPT: A program to produce both detailed and schematic plots of protein structures, *J. Appl. Crystallogr. 24*, 946−950.
28. Merritt, E. A., and Bacon, D. J. (1997) Raster3D: Photorealistic molecular graphics, *Methods Enzymol. 277*, 505−524.
29. Kitagawa, T., and Hirota, S. (2002) in *Handbook of vibrational spectroscopy 5* (Chalmers, J. M., and Griffiths, P. R., Eds.) pp 3426−3446, Johns Willey & Sons, Chichester, U.K.
30. Ray, G. B., Li, X.-Y., Ibers, J. A., Sessler, J. L., and Spiro, T. G. (1994) How far can proteins bend the FeCO unit? Distal polar and steric effects in heme proteins and models, *J. Am. Chem. Soc. 116*, 162−176.
31. Luzzati, P. V. (1952) Traitement statistique des erreurs dans la determination des structures cristallines, *Acta Crystallogr. 5*, 802−810.
32. Brucker, E. A., Olson, J. S., Phillips, G. N., Jr., Dou, Y., and Ikeda-Saito, M. (1996) High resolution crystal structures of the deoxy, oxy, and aquomet forms of cobalt myoglobin, *J. Biol. Chem. 271*, 25419−25422.
33. Kincaid, J. R. (2000) in *The Porphyrin Handbook* (Kadish, K. M., Smith, K., and Guilard, K. S., Eds.) Vol. 7, pp 225−291, Academic Press, San Diego.
34. Shimada, H., and Caughey, W. S. (1982) Dynamic protein structures, *J. Biol. Chem. 257*, 11893−11900.
35. Li, T., Quillin, M. L., Phillips, G. N., Jr., and Olson, J. S. (1994) Structural determinants of the stretching frequency of CO bound to myoglobin, *Biochemistry 33*, 1433−1446.
36. Hayashi, T., Nakagawa, T., Harada, K., Matsuo, T., Hitomi, Y., and Hisaeda, Y. (2004) Chemical properties of sperm whale myoglobins reconstituted with monopropionate hemins, *Chem. Lett. 33*, 1512−1513.
37. La Mar, G. N., Emerson, S. D., Lecomte, J. T. J., Pande, U., Smith, K. M., Craig, G. W., and Kehres, L. A. (1986) Influence of propionate side chains on the equilibrium heme orientation in sperm whale myoglobin. Heme resonance assignments and structure determination by nuclear Overhauser effect measurement, *J. Am. Chem. Soc. 108*, 5568−5573.
38. Yamamoto, Y., Nanai, N., Chujo, R., and Suzuki, T. (1990) Heme methyl hyperfine shift pattern as a probe for determining the orientation of the functionally relevant proximal histidyl imidazole with respect to the heme in hemoproteins, *FEBS Lett. 264*, 113−116.
39. Peterson, E. S., Friedman, J. M., Chien, E. Y. T., and Sligar, S. G. (1998) Functional implications of the proximal hydrogen-bonding network in myoglobin: A resonance Raman and kinetic study of Leu89, Ser92, His97, and F-helix swap mutants, *Biochemistry 37*, 12301−12319.
40. Brantley, R. E., Jr., Smerdon, S. J., Wilkinson, A. J., Singleton, E. W., and Olson, J. S. (1993) The mechanism of autoxidation of myoglobin, *J. Biol. Chem. 268*, 6995−7010.
41. Gonzalez, G., Gilles-Gonzalez, M. A., Rybak-Akimova, E. V., Buchalova, M., and Busch, D. H. (1998) Mechanisms of autoxidation of the oxygen sensor FixL and *Aplysia* myoglobin implications for oxygen-binding heme proteins, *Biochemistry 37*, 10188−10194.
42. Shikama, K. (1998) The molecular mechanism of autoxidation for myoglobin and hemoglobin: A venerable puzzle, *Chem. Rev. 98*, 1357−1373.
43. Olson, J. S., and Phillips, G. N., Jr. (1996) Kinetic pathways and barriers for ligand binding to myoglobin, *J. Biol. Chem. 271*, 17593−17596.

BI7007068